Bibliographical reference

Timoshenko Modeling of the Pipa String, Shin-Hui Lin Chin and Charles Steele, Acta Acustica **vol. 97** (Number 2), 2011, pp. 315-324

DOI

https://doi.org/10.3813/AAA.918411

Acta Acustica united with Acustica
Vol. 97 (2011) 315 – 324

DOI 10.3813/AAA.918411

Timoshenko Modeling of the Pipa String

Shin-Hui Lin Chin[1)], Charles Steele[2)]

[1)] Center for Computer Research in Music and Acoustics, Stanford University, Stanford, California, 95405-8180, USA. sandylin@ccrma.stanford.edu

[2)] Department of Mechanical Engineering, Stanford University, Stanford, California, 95405-8180

Summary

The timbre of the pipa, a traditional plucked Chinese music instrument, is characterized by nuanced inharmonicity resulting from peculiarities of regionally distinct string composition and construction. This paper investigates the relationship between string physical construction and the resulting inharmonicity in the sounds produced by the traditional silk and modern Beijing and Shanghai metallic strings. Inharmonicity occurs in string instruments primary due to stiffness of the strings, and is commonly analyzed using Fletcher's inharmonicity formulation based on the Euler-Bernoulli stiff-string physical model. While this formulation accurately predicts partial shifts observed in the solid-core steel Beijing strings throughout the audible frequency range, it fails to accurately predict the partial shifts observed in the stranded-core steel Shanghai and traditional silk strings beyond about 8 kHz. An alternate formulation of inharmonicity is developed based on the Timoshenko beam physical model, which accounts for not only stiffness, but also rotary inertia and shear deformation within the string. Inharmonic partials derived from this formulation are verified by comparing against spectra of pipa recordings, and it is found that the Timoshenko-based formulation is capable of predicting the observed inharmonicity across all pipa string types. The unusual inharmonicity of the silk and Shanghai strings above 8 kHz is explained by the shear deformation properties of the string materials and construction, which limit the phase velocities supported by the strings and hence limit the inharmonic frequency shifts of the upper partials. In the case of the solid-core steel Beijing string, the shear deformation limit is beyond the audible frequency range, so the Euler-Bernoulli based formulation is adequate to explain its inharmonicity. In the case of the stranded steel Shanghai and twisted silk strings, whose physical shear moduli are 1-2 orders of magnitude smaller than that of the solid-core steel Beijing string, the shear deformation influences inharmonicity within the audible frequency range. For these strings (and generally for strings with relatively lower shear moduli), the Timoshenko-based formulation of inharmonicity should be used.

PACS no. 43.40.Cw, 43.75.Gh

1. Introduction

The pipa, a four-stringed instrument resembling a lute (Figure 1), has played an essential role in Chinese orchestra for hundred of years, reaching its peak in popularity during the Sui and Tang dynasty (581-907 AD) where it played a central role in *yen-yüeh* or court banquet music [1]. The pipa provides the main melody in the Chinese orchestral ensemble as well as the Chinese silk chamber ensemble. The traditional pipa strings are made of twisted silk, but modern pipa strings are predominately made of steel, with outer coverings of copper, nickel or nylon. The change in string materials and construction has resulted in profound changes in timbre. This effect is so great that differences in pipa string construction between the two major regions of manufacture, Shanghai and Beijing, have given rise to different musical repertoire tailored to the characteristics of each region's strings.

Figure 1. Modern pipa.

A key aspect of the timbre differences is the degree of inharmonicity in the strings. A moderate amount of inharmonicity creates a sense of warmth, but an excessive amount of inharmonicity can result in a harsher metallic sound [2]. As a common example, a grand piano has less inharmonicity than an upright piano, and is generally regarded as producing a more pleasing sound [3]. In the case of the pipa, musicians tend to prefer the silk or Shanghai

Received 18 January 2010,
accepted 12 January 2011.

strings over the Beijing strings, which have a more metallic sound [4, 5]. Inharmonicity influences pitch perception [6, 7], and has been extensively studied as an important consideration for synthesis of many stringed instruments, such as the kantele [8], harpsichord [9], guqin [10] and guitar [11].

Physically, inharmonicity is caused by non-ideal mechanical properties of the string material and produces partials which are non-integer multiples of the string's fundamental frequency. Much of the analysis of string inharmonicity to date is based upon Fletcher's formulation of the Euler-Bernoulli string model [2], which accounts for stiffness in the string. When applied to the solid-core Beijing pipa strings, Fletcher's formulation accurately predicts the inharmonicity throughout the audible spectrum. However, when applied to the stranded Shanghai pipa strings, Fletcher's formulation matches the inharmonicity only in the lower partials, and fails to accurately predict the inharmonicity in higher partials beyond about 8 kHz.

The purpose of this paper is to explore the relationship between string physical construction and the resulting inharmonicity and timbre differences in the sounds produced by the silk, Beijing and Shanghai pipa strings. First, the physical construction of the different pipa strings is examined. Second, Fletcher's inharmonicity formulation of the Euler-Bernoulli string model is reviewed. Finally, an alternate inharmonicity formulation based on the Timoshenko beam model is developed which better explains the inharmonicity of the higher partials of the Shanghai strings.

2. Structure of the pipa strings

Contemporary pipa strings are made in two distinct ways depending on the place of manufacture, Shanghai or Beijing. Each Shanghai pipa string is made of seven steel strings wound together within a helical coil of covering copper, except the A3 (221 Hz) string which is not covered with copper. Every Shanghai string is wound with an outer surface of plastic. In contrast, the Beijing A3 string is made of only one steel string. The remaining three Beijing strings contain one steel string core, covered with nickel. Contemporary repertoire is predominately played using either all Shanghai strings, or a Beijing A3 string plus three Shanghai strings due to the heavy metallic sound of the other Beijing strings.

Microphotographs of Shanghai strings are shown in Figures 2 and 3. These pictures were made using a Nikon SMZ 1500 microscope and a Sony DSC S75 digital camera. The pipa strings share a superficial similarity to the well-studied piano strings, which typically consist of a tensioned steel core wire, around which is wound a helical coil of covering wire. In the case of the piano, the covering wire adds mass with only 5-7% increase in stiffness [12]. As will be shown in the physical modeling section, in the case of the pipa, the covering wire is a significant contributor to stiffness and cannot be neglected.

The diameter of each steel strand is measured using a Union Hisomet measuring microscope (±0.1μm precision). The final strand radius r is calculated from the average of three measured steel strands for each type of string. The outer and inner diameters of the copper covering wire are also measured withe the same microscope, and the corresponding radii (a and b, respectively) are recorded. The mass of each string is measured using a Mettler Toledo micro balance (model AB 204, ±0.1mg precision), and the mass per unit length ρ_{lin} is recorded. A summary of string parameters is given in Table I.

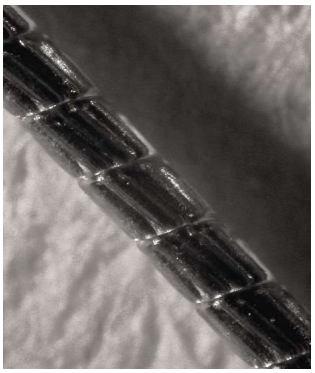

Figure 2. Shanghai first string (A3 221 Hz) microphotograph. Unlike the other three Shanghai strings, the first string is made of seven steel strands wound together without a copper cover.

Figure 3. Shanghai second string microphotograph cross-section with plastic cover removed.

The effective moment of inertia of the seven-strand core shown in Figure 4 can be computed by applying the parallel-axis theorem to compute the moment of inertia contribution of the off-axis strands. The moment of inertia of a cross section of area A about the x axis is

$$\bar{I}_x = \int y^2 \, \mathrm{d}A. \tag{1}$$

From the parallel-axis theorem, the moment of inertia about the non-centroidal x axis is given by

$$I_x = \bar{I}_x + A d_x^2, \tag{2}$$

where $A = \pi r^2$ is the cross sectional area of one steel strand and $d_x = r\sqrt{3}$ is the distance from the object centroid to the axis. The cumulative moment of inertia for all

Table I. Measured and computed string parameters.

		Beijing A3	Shanghai A3	Shanghai E2	Shanghai D2	Shanghai A2
Measured parameters						
Fundamental Frequency, f_0	[Hz]	221.0	221.0	166.7	147.3	110.5
String length, L	[m]	0.734	0.734	0.734	0.734	0.734
Copper, outer radius, a	[μm]	-	-	193.2	284.6	393.8
Copper, inner radius, b	[μm]	-	-	142.5	151.5	180
Number of steel strands		1	7	7	7	7
Steel strand radius, r	[μm]	124.5	39.8	47.4	50.5	60.4
Linear Mass Density, ρ_{lin}	[g/m]	0.385	0.42	1.015	1.59	3.088
Material Properties						
Young's modulus, copper, E_{copper}	[GPa]	-	-	100	100	100
Young's modulus, steel, E_{steel}	[GPa]	200	200	200	200	200
Shear modulus, steel, G_{steel}		79.3 GPa (solid)	153.8 MPa (stranded)	153.8 MPa (stranded)	153.8 MPa (stranded)	153.8MPa (stranded)
Calculated parameters						
Moment of Inertia, Copper, I_{copper}	[kg/m^2]	-	-	$7.69 \cdot 10^{-16}$	$4.74 \cdot 10^{-15}$	$1.81 \cdot 10^{-14}$
Moment of Inertia, Steel, I_{steel}	[kg/m^2]	-	-	$2.20 \cdot 10^{-16}$	$2.81 \cdot 10^{-16}$	$5.60 \cdot 10^{-16}$
Tension, T	[N]	40.5	44.2	60.1	74.4	81.3

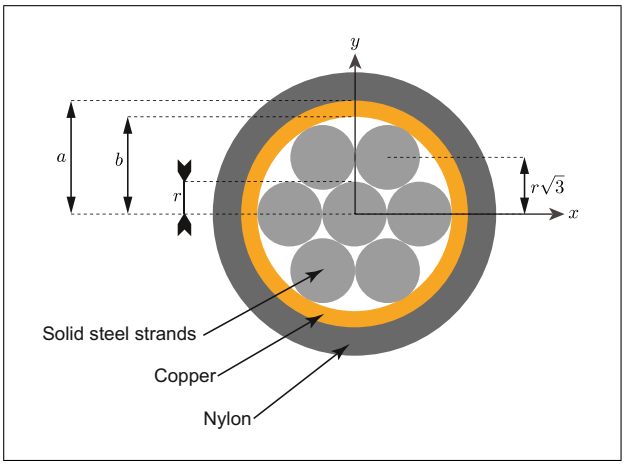

Figure 4. Shanghai string construction, cross section.

steel strands is the sum of the three on-axis strand and four off-axis strand moments of inertia,

$$I_{steel} = 3\bar{I}_x + 4I_x. \tag{3}$$

The copper cover is on-axis, so can be computed from the cylindrical wire equation as

$$I_{copper} = \pi \frac{a^4 - b^4}{4}, \tag{4}$$

where a and b are the outer and inner radii of the copper cover, respectively.

The calculated moments of inertia computed for the pipa strings are given at the bottom of Table I. For the larger three Shanghai strings, the copper covering wire is a significant contributor to the overall moment of inertia of the strings.

3. Derivation of inharmonicity for the pipa strings

3.1. Euler-Bernoulli stiff string formulation

The following equation describes the transverse motion of strings, including the effects of bending stiffness.

$$EI\frac{\partial^4 y}{\partial x^4} - T\frac{\partial^2 y}{\partial x^2} - \rho_{lin}\frac{\partial^2 y}{\partial t^2} = 0. \tag{5}$$

The first term is the contribution from stiffness; the second term is the contribution from tension. In the equation, y is the transverse string displacement; x is the position along the string; t is the time; ρ_{lin} is mass per unit length; T is tension; E is Young's modulus; I is the moment of inertia. The steel alloy used in the pipa strings is common stainless steel; the conventional values for Young's modulus for stainless steel and copper (given in Table I) are used for pipa string calculations.

Following the method of Fletcher *et al.* [2], the frequency of stretched partials can be derived. The string is simply supported at both ends, which corresponds to the following boundary conditions:

$$\begin{cases} y(0,t) = y(L,t) = 0, \\ \dfrac{\partial^2 y}{\partial x^2}(0,t) = \dfrac{\partial^2 y}{\partial x^2}(L,t) = 0. \end{cases} \tag{6}$$

The general solution to this system is

$$y = Ae^{j\omega t}\sin\frac{n\pi x}{L}, \qquad n = 1, 2, 3, \ldots. \tag{7}$$

Substituting these into the string equation produces

$$\left(EI\left(\frac{n\pi}{L}\right)^4 + T\left(\frac{n\pi}{L}\right)^4 - \rho_{lin}\omega_n^2\right) y = 0. \tag{8}$$

Table II. Computed inharmonicity coefficients B from each of the Euler-Bernoulli models, compared to fitted inharmonicity coefficients of recorded signal spectra between 0 and 5 kHz.

String	Solid steel core	7-strand steel core	7-strand steel core plus copper	Measured from spectrum
Beijing A3	$1.71 \cdot 10^{-5}$	-	-	$1.50 \cdot 10^{-5}$
Shanghai A3	$1.35 \cdot 10^{-5}$	$9.17 \cdot 10^{-6}$	-	$2.60 \cdot 10^{-5}$
Shanghai E2	$1.97 \cdot 10^{-5}$	$1.34 \cdot 10^{-5}$	$3.69 \cdot 10^{-5}$	$2.60 \cdot 10^{-5}$
Shanghai D2	$2.04 \cdot 10^{-5}$	$1.38 \cdot 10^{-5}$	$1.31 \cdot 10^{-4}$	$2.40 \cdot 10^{-5}$
Shanghai A2	$3.72 \cdot 10^{-5}$	$2.52 \cdot 10^{-5}$	$4.33 \cdot 10^{-4}$	$3.60 \cdot 10^{-5}$

Resonant frequencies occur at

$$\rho\omega_n^2 = T\left(\frac{n\pi}{L}\right)^2 + EI\left(\frac{n\pi}{L}\right)^4. \tag{9}$$

If $T = 0$,

$$\begin{aligned} \omega_n &= \sqrt{\frac{EI}{\rho}}\left(\frac{\pi}{L}\right)n^2, \qquad n = 1, 2, 3, \ldots, \\ \omega_1 &= \sqrt{\frac{EI}{\rho}}\left(\frac{\pi}{L}\right),\ \omega_2 = 4\omega_1,\ \omega_3 = 9\omega_2, \ldots. \end{aligned} \tag{10}$$

If $T > 0$, equation (9) can be rewritten as

$$\omega_n = \sqrt{\left(\frac{n\pi}{L}\right)^2\left(\frac{T}{\rho}\right)\left(1 + \frac{EI}{T}\left(\frac{n\pi}{L}\right)^2\right)} \tag{11}$$

$$= n\frac{\pi}{L}\sqrt{\frac{T}{\rho}}\sqrt{1 + \left(\frac{EI\pi^2}{TL^2}\right)n^2}. \tag{12}$$

Using the substitutions

$$\omega_n = 2\pi f_n, \quad B \triangleq \frac{EI\pi^2}{TL^2}, \quad f_0 \triangleq \frac{1}{2L}\sqrt{\frac{T}{\rho}}, \tag{13}$$

where B is the inharmonicity coefficient and f_0 is the fundamental frequency of the string without stiffness, the frequency of the n^{th} partial is

$$f_n = nf_0\sqrt{1 + Bn^2}, \qquad n > 0. \tag{14}$$

The final equations (13) and (14) give the fundamental frequency and inharmonic shift of upper partials in terms of physical and material parameters.

Based on these equations and the measured physical parameters (summarized in Table I), the effective inharmonicity coefficients for the commonly used Beijing and Shanghai strings are given in Table II.

The spectrum of the A221 Shanghai string recording is shown in Figure 5 (please see appendix for details on the spectral analysis and method for extracting empirical inharmonic partials). The harmonics of the pipa sound are not exact integral multiples of the fundamental frequency. The string's stiffness increases the frequencies of the higher partials, which are noticeably higher than ideal harmonic frequencies beyond about 5 kHz. Also, as the

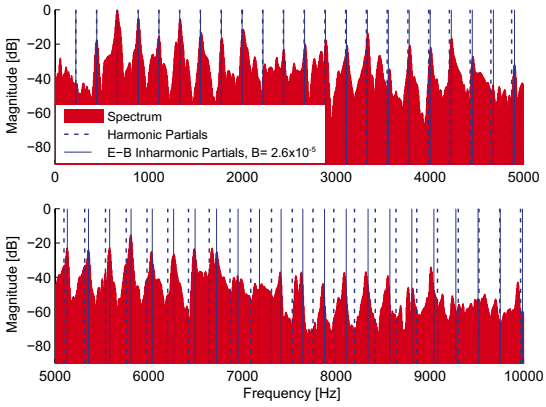

Figure 5. Comparison of stiff-string inharmonicity versus the spectrum of a Shanghai string recording (A3 $f_0 = 221$ Hz). Dashed vertical bars indicate positions of ideal harmonic overtones; solid vertical bars indicate positions of inharmonic partials predicted by Fletcher's formulation with $B = 2.6 \cdot 10^{-5}$. Predictions match the recorded spectrum through about 5 kHz, but diverge beyond 8 kHz.

value of inharmonicity coefficients increase, greater shifts are seen in upper partial frequencies. The Euler-Bernoulli model accurately predicts the frequencies of the lower partials, but overestimates the frequencies of higher partials of the Shanghai and Silk strings. Example of partial frequency shifts for various approximations of B for the Shanghai A3 string are shown in Figure 6.

For reference, a comparison of selected pipa string parameters with piano string data from [13] is given in Table III. The cross section area (and therefore linear mass density) of piano strings is roughly an order of magnitude larger than that of pipa strings. Following the f_0 relationship in equation (9) the tension necessary to tune the piano strings to the C3-C4 range is consequently an order of magnitude larger than that of the pipa. Applying a cylindrical approximation for all strings,

$$B = \left.\frac{EI\pi^2}{TL^2}\right|_{I=A^2/4\pi} = \frac{E\pi}{L^2}\frac{A^2}{T}, \tag{15}$$

and considering the order of magnitude differences in cross section area A and tension T, the resulting inharmonicity B of the piano strings is likewise an order of magnitude larger than that of the pipa strings.

Table III. Comparison of pipa and piano strings. Piano values are based on data published by [13].

Strings	Frequency [Hz]	String length [m]	cross-section area A [mm^2]	Tension [N]	Inharm. Coef. B
Piano C2	65	1.232	0.908	952.6	$8.725 \cdot 10^{-5}$
Piano C3	131	1.187	0.908	687.1	$1.3032 \cdot 10^{-4}$
Piano C4	262	0.649	0.825	747.0	$3.3144 \cdot 10^{-4}$
Shanghai A3	221	0.734	0.0348	44.2	$2.60 \cdot 10^{-5}$
Beijing A3	221	0.734	0.0487	40.5	$1.50 \cdot 10^{-5}$

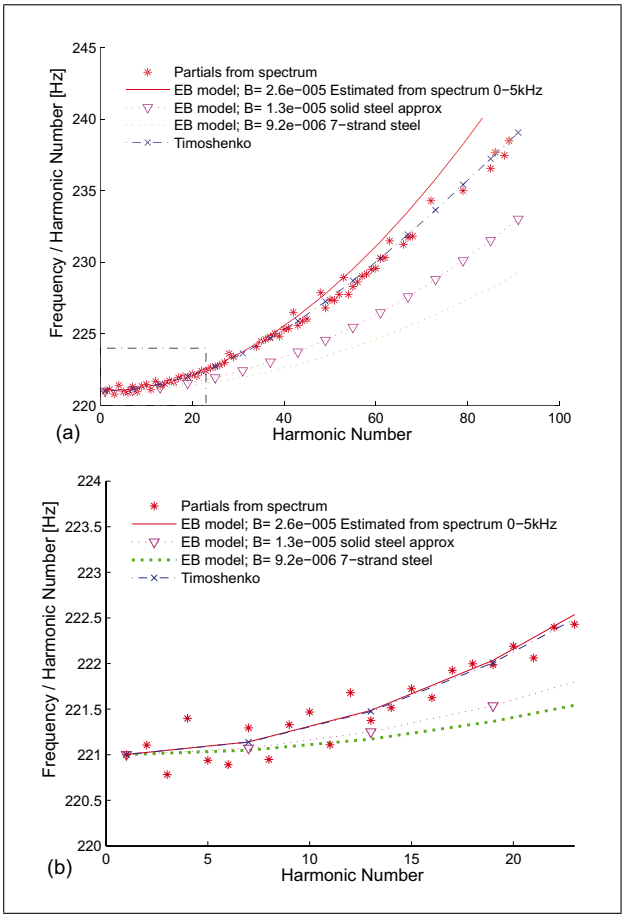

Figure 6. Partial frequencies f_n divided by partial number n, based on several possible inharmonicity coefficient values of simplified models for the Shanghai A3 (221 Hz) string. The curve marked with asterisks shows the inharmonicity corresponding to partials extracted from spectral analysis of a pipa recording. Plot (a) shows the partials extracted from the full spectrum. Plot (b) is a detailed view of the marked rectangular region from (a) which shows the lower partials (< 5 kHz) used to estimate the coefficient of inharmonicity B.

3.2. Timoshenko Beam formulation, including shear force and rotational motion

We reconsider the behavior of waves and vibrations on the pipa strings assuming the string is composed of Timoshenko beam elements, which include the effects of not only stiffness (as in the Euler-Bernoulli model) but also rotary inertia (as in the Rayleigh model) and shear deformation [14]. As shown in Figure 7, shear stress on the

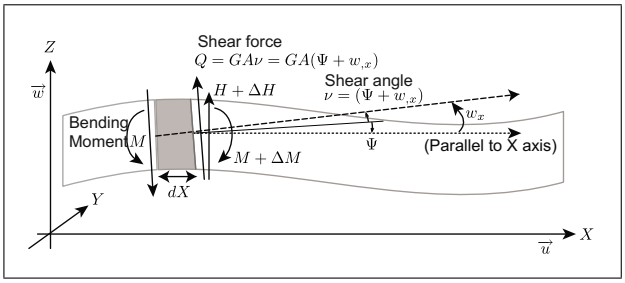

Figure 7. Forces and bending moments acting upon a differential element of the string. In the Timoshenko beam formulation, the differential element is subject to shear deformation: the slope of the transverse displacement $w_{,x}$ (dashed line through the center of the left and right faces) is no longer aligned to the slope of bending Ψ (perpendicular to face), but forms a shear angle $\nu = (\Psi + w_{,x})$ which results in a shear force $V = GA\nu = GA(\Psi + w_{,x})$ parallel to the face.

cross-section elements causes the section to no longer be perpendicular to the neutral axis. In this figure, Ψ is used to measure the slope of the cross-section due to the effects of bending and ν is the contribution due to shear deformation. The resulting slope of the centroidal axis $w_{,x}$ (where $[\cdot]_{,x}$ indicates the partial derivative with respect to x) due to bending shear is given by

$$w_{,x} = \frac{\partial Z}{\partial X} = \nu - \Psi. \tag{16}$$

The shear force at the cross-section is given in terms of the shear strain as

$$V = G \int_A \nu \, \mathrm{d}A = GA\nu. \tag{17}$$

The action of this mechanical system is defined by the integral of the system's Lagrange function

$$\Pi = \int_0^l L(\Psi, w, u) \, \mathrm{d}x. \tag{18}$$

By the principle of least action,

$$\delta\Pi = 0. \tag{19}$$

This is satisfied if and only if the Euler-Lagrange equations for the system hold

$$\begin{cases} -\left(\frac{\partial L}{\partial \dot{\Psi}}\right) - \left(\frac{\partial L}{\partial \Psi_{,x}}\right)_{,x} + \frac{\partial L}{\partial \Psi} = 0, \\ -\left(\frac{\partial L}{\partial w_{,x}}\right)_{,x} + \frac{\partial L}{\partial w} = 0, \\ -\left(\frac{\partial L}{\partial u_{,x}}\right)_{,x} + \frac{\partial L}{\partial u} = 0. \end{cases} \tag{20}$$

For the Timoshenko beam, the action integral for the system is

$$\Pi = \int_0^l \left\{ \left[\frac{1}{2} EI\Psi_{,x}^2 + \frac{1}{2} EA \left(u_{,x} + \frac{1}{2} w_{,x}^2 \right)^2 + \frac{1}{2} GA \left(\Psi + w_{,x} \right)^2 \right] - pw - p_s u \right\} \mathrm{d}x. \tag{21}$$

This equation has five terms in units of energy: potential energy due to elastic deformation, tension and shear deformation, and kinetic energy due to translation and rotation. Note that neglecting the shear deformation term yields the Rayleigh model, and that neglecting both the shear deformation and rotational kinetic energy term yields the Euler-Bernoulli model.

Applying the Euler-Lagrange equations in each of the coordinates Ψ, w and u gives

$$\Psi: \quad -\left(EI\Psi_{,x}\right)_{,x} + GA\left(\Psi + w_{,x}\right) = 0, \tag{22}$$

$$w: \quad -\left\{ EA\left(u_{,x} + \frac{1}{2} w_{,x}^2 \right) + GA\left(\Psi + w_{,x}\right) \right\} - p = 0, \tag{23}$$

$$u: \quad -\left\{ EA\left(u_{,x} + \frac{1}{2} w_{,x}^2 \right) \right\} - p_s = 0. \tag{24}$$

The normal force can be defined as

$$N \triangleq EA\left(u_{,x} + \frac{1}{2} w_{,x}^2 \right), \tag{25}$$

and the total of normal force and shear force can be defined as

$$H \triangleq N w_{,x} + GA(\Psi + w_{,x}). \tag{26}$$

The bending moment is

$$M = EI\Psi_{,x} \iff \Psi_{,x} = \frac{M}{EI}. \tag{27}$$

Solving (26) for $w_{,x}$

$$w_{,x} = \frac{-\Psi + \frac{H}{GA}}{1 + \frac{N}{GA}}. \tag{28}$$

For convenience we define

$$\gamma \triangleq \frac{1}{1 + \frac{N}{GA}}. \tag{29}$$

We summarize the key equations below

$$\begin{cases} M_{,x} = \gamma H + N\gamma\Psi + p_s = \gamma H + N\gamma\Psi + \rho A\ddot{\Psi}, \\ H_{,x} = -p = \rho A\ddot{w}, \\ \Psi_{,x} = \frac{M}{EI}, \\ w_{,x} = \frac{\gamma}{GA} H - \gamma\Psi, \end{cases} \tag{30}$$

or rewriting in matrix form as

$$\begin{pmatrix} M \\ H \\ \Psi \\ w \end{pmatrix}_{,x} = \begin{pmatrix} 0 & \gamma & N\gamma & 0 \\ 0 & 0 & 0 & 0 \\ \frac{1}{EI} & 0 & 0 & 0 \\ 0 & \frac{\gamma}{GA} & -\gamma & 0 \end{pmatrix} \begin{pmatrix} M \\ H \\ \Psi \\ w \end{pmatrix} + \begin{pmatrix} \rho I\ddot{\Psi} \\ \rho A\ddot{w} \\ 0 \\ 0 \end{pmatrix}. \tag{31}$$

The characteristic equation

$$det \left| ki\mathbb{I} - \begin{pmatrix} 0 & \gamma & N\gamma - I\rho\omega^2 & 0 \\ 0 & 0 & 0 & -A\rho\omega^2 \\ \frac{1}{EI} & 0 & 0 & 0 \\ 0 & \frac{\gamma}{GA} & -\gamma & 0 \end{pmatrix} \right| = 0, \tag{32}$$

gives the dispersion relation

$$\underbrace{k^4 + \frac{k^2 T\gamma}{EI} - \frac{A\gamma^2\rho\omega^2}{EI}}_{Euler-Bernoulli} - \underbrace{\frac{k^2\rho\omega^2}{E}}_{Rayleigh} - \underbrace{\frac{k^2\gamma\rho\omega^2}{G} - \frac{T\gamma^2\rho\omega^2}{EIG} - \frac{\gamma\rho^2\omega^4}{EG}}_{Timoshenko} = 0, \tag{33}$$

where k is the wavenumber, $i = \sqrt{-1}$ and $\mathbb{I}$ is the identity matrix. Note that if rotary inertia (of the Rayleigh model) and shear deformation (of the Timoshenko model) contributions are neglected, the dispersion relation (33) reduces to equation (9) of the Euler-Bernoulli model (where $k = n\pi/L$ and $\gamma = 1$).

Using the following substitutions,

$$\omega = kv, \quad E = c_1^2\rho, \quad G = c_2^2\rho, \tag{34}$$

where c_1 and c_2 are the longitudinal and shear wave speeds, respectively,

$$c_1 \triangleq \sqrt{\frac{E}{\rho}}, \qquad c_2 \triangleq \sqrt{\frac{G}{\rho}}, \tag{35}$$

and solving equation (33) for k^2 gives

$$k^2 = \frac{-c_2^2 T\gamma - Tv^2\gamma^2 + Ac_2^2 v^2\gamma^2\rho}{I\rho\left(c_1^2 + v^2\right)\left(-c_2^2 + v^2\gamma\right)}. \tag{36}$$

Table IV. Predicted partials from ideal string f_I, the Euler-Bernoulli stiff string f_{EB} and Timoshenko beam models f_T for the Shanghai A3 string. The difference between the predicted partial for each model and the ideal harmonic is also given.

Partial	Ideal f_I [Hz]	Euler-Bernoulli f_{EB} [Hz]	Euler-Bernoulli $f_{EB} - f_I$ [Hz]	Timoshenko f_T [Hz]	Timoshenko $f_T - f_I$ [Hz]
1	221.0	221.0	+0.0	221.0	+0.0
2	442.0	442.0	+0.0	442.0	+0.0
3	663.0	663.0	+0.0	663.0	+0.0
4	884.0	884.1	+0.1	884.1	+0.1
5	1105.0	1105.1	+0.1	1105.1	+0.1
10	2210.0	2211.0	+1.0	2211.0	+1.0
20	4420.0	4428.1	+8.1	4428.8	+7.8
30	6630.0	6657.3	+27.3	6655.1	+25.1
40	8840.0	8905.6	+64.6	8896.3	+56.3
50	11050.0	11175.9	+125.9	11152.8	+102.8

The Timoshenko model phase velocity relationship can be obtained by solving equation (36) for phase velocity v in terms of wavenumber k.

$$v^2(k) = \frac{c_1^2}{2} + \frac{c_2^2}{2\gamma} + \frac{Ac_2^2\gamma}{2Ik^2} + \frac{T\gamma}{2I\rho k^2} \pm \left[-4I\gamma\rho k^2\left(c_2^2 T\gamma + c_1^2 c_2^2 I\rho k^2\right) + \left(-T\gamma^2 - Ac_2^2\gamma^2\rho - c_2^2 I\rho k^2 - c_1^2 I\gamma\rho k^2\right)^2\right]^{1/2}\left[2Ik^2\gamma\rho\right]^{-1}. \quad (37)$$

The corresponding Euler-Bernoulli phase velocity (v_{EB}) relationship can be obtained in a similar manner, and is given below.

$$v_{EB}^2(k) = \frac{T}{\rho A} + c_1^2\frac{I}{A}k^2. \quad (38)$$

The positive phase velocities of equations (37) and (38) are plotted in Figure 8. For large wavenumbers, the Euler-Bernoulli model phase velocity increases without bound, while the Timoshenko model phase velocity is limited by shear deformation c_2.

The frequency of the n^{th} inharmonic partial f_n can be obtained by solving equation (37) in terms of radial frequency ω

$$\omega_T^2(k) = \frac{1}{2I\gamma\rho^2}\Big(I\rho k^2(E\gamma + G) + T\gamma^2\rho + GA\gamma^2\rho \pm \left[-4I\gamma\rho^2 k^2\left(EGIk^2 + GT\gamma\right) + \left(I\rho k^2(E\gamma + GI) + T\gamma^2\rho + GA\gamma^2\rho\right)^2\right]^{1/2}\Big), \quad (39)$$

and using the relationship

$$f_n = \left.\frac{\omega(k)}{2\pi}\right|_{k=\frac{n\pi}{L}}, \qquad n = 1, 2, 3, \ldots . \quad (40)$$

For the Shanghai A3 pipa string with physical parameters listed in Table I, the inharmonic partial shifts predicted by the Euler-Bernoulli and Timoshenko models can be seen in Figures 9 and 10. Computed numeric values for selected predicted partials using both models are given in Table IV.

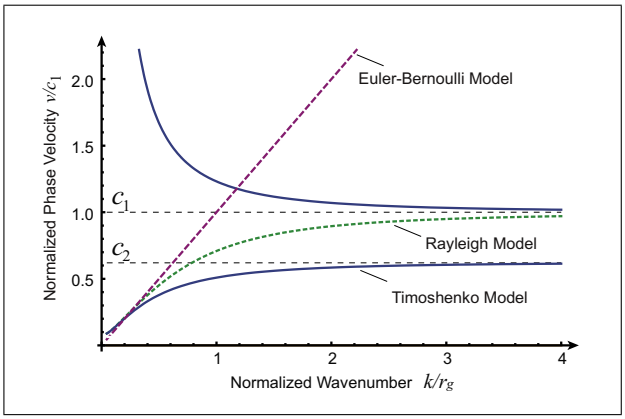

Figure 8. Phase velocity relationships for Timoshenko (solid), Rayleigh (dotted) and Euler-Bernoulli (dashed) string models. Phase velocity is normalized to the longitudinal wave speed c_1, and wavenumber is normalized to the radius of gyration $r_g = \sqrt{I/A}$.

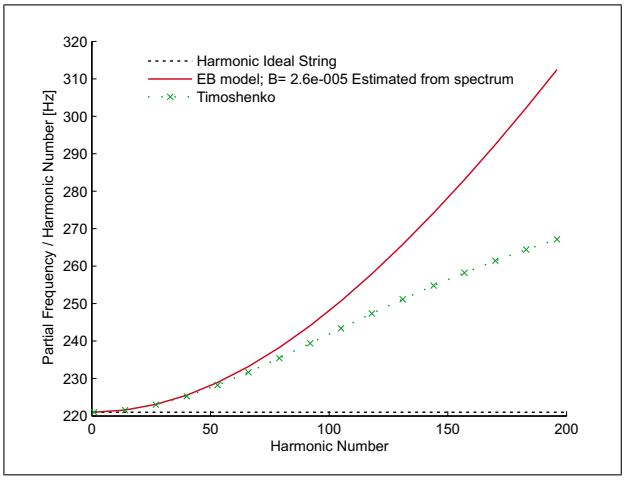

Figure 9. Partial shift due to inharmonicity for the Shanghai A3 (221 Hz) string, as predicted by different physical models.

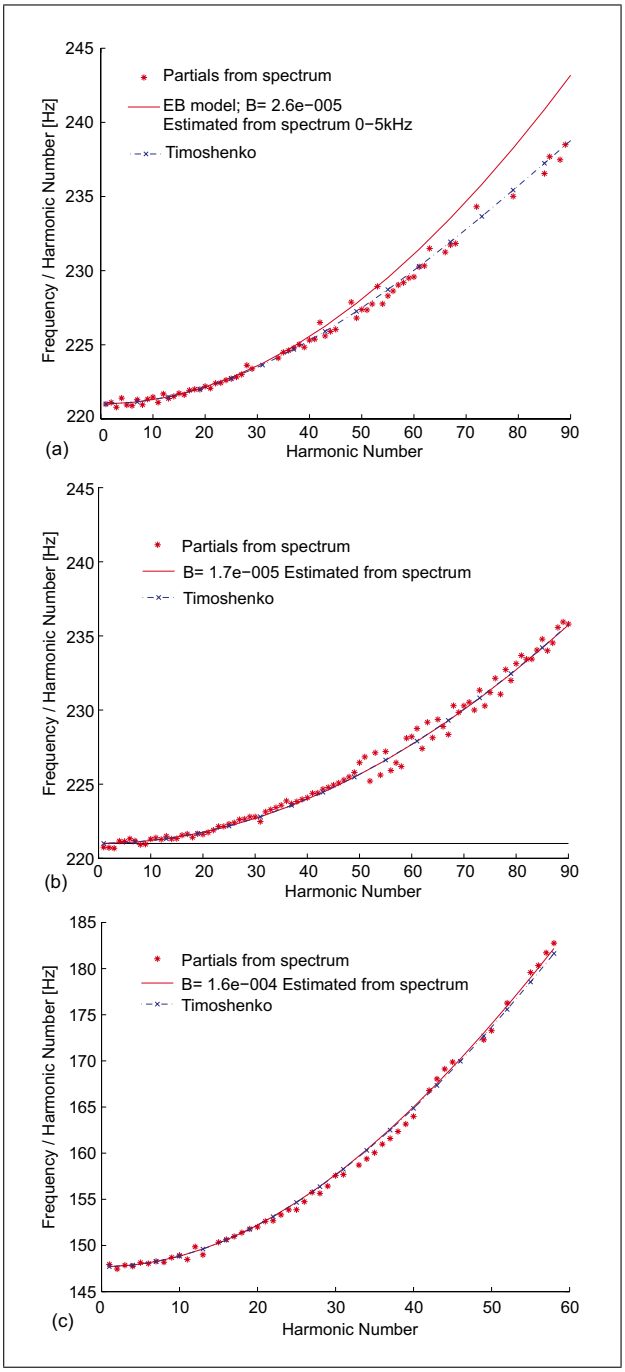

Figure 10. Comparison of Euler-Bernoulli, Timoshenko and measured partial shifts for (a) Shanghai A3 (221 Hz) stranded-core steel string, (b) Beijing A4 (221 Hz) solid-core steel string, and (c) silk D3 (147.4 Hz) string.

For lower partials, the Timoshenko model agrees with Fletcher's formulation. For higher partials above about 8 kHz, the partial shift predicted by the two models diverge.

Unlike the Euler-Bernoulli formulation in the previous section, the Timoshenko beam formulation has a bounded phase velocity at high frequencies, which limits the frequency shift of inharmonic partials at high frequencies. Insight into the high-frequency dispersion behavior of the Timoshenko model can be obtained by examining the limits of the wavenumber-phase velocity equation (36). At the short wavelength limit $k \to \infty$, the phase velocity v approaches a limit dominated by shear deformation c_2.

In the case of the pipa, the distinctive seven-stranded core gives the Shanghai pipa strings a shear modulus G which is two orders of magnitude smaller than that of typical solid-core strings (79.3 GPa for solid steel as in the Beijing strings, 44.7GPa for solid copper, or 40.1 GPa for solid brass, compared with 153.8 MPa for stranded steel as in the Shanghai strings or 3GPa for silk). For the pipa strings, the effect on inharmonicity becomes significant within the range of hearing.

4. Conclusion

In this paper, the structure of pipa strings has been analyzed. The hypothesis which motivated this work is that the pipa string structure is a main contributor to the pipa's characteristic inharmonicity and timbral sound. Owing to its distinctive string structures, the calculation of pipa inharmonicity is investigated using physical models based on both the conventional Euler-Bernoulli stiff string formulation and Timoshenko beam formulation. From the physical models developed in this paper, it is clear that the inharmonicity-limiting effect of shear deformation is the key difference between the more metallic Beijing strings and the warmer silk and Shanghai strings.

Further, the analysis of the Timoshenko-based model suggests the following guideline can be used for computing inharmonicity for a string: for solid core strings made from steel, copper, bronze, or similar materials, Fletcher's formulation based upon the Euler-Bernoulli stiff-string model is most likely sufficient to model the inharmonicity of audible partials. However, for stranded core strings or strings made with materials with small shear moduli (notably silk at 3GPa, or nylon at 4.1GPa), high partials may be audibly affected by the shear deformation phase velocity limit, so the Timoshenko-based formulation should be used.

Appendix

A1. Spectral Analysis

In order to obtain the empirical inharmonic partials for this investigation, performances of the Beijing and Shanghai plucked open strings were recorded at 16 bit resolution and 44100 Hz sampling frequency, and analyzed to extract partial frequencies. The silk string recording was obtained separately, and was sampled at 16 bit resolution and 22050 Hz. Open strings were chosen instead of fretted strings in order to minimize the influence of left hand fingering technique, which could otherwise introduce pitch drift or other unwanted artifacts.

The key components of the analysis are illustrated in Figure A1. A short-time Fourier analysis approach was used to compute a spectrogram of each recording (4096-point Hanning window, zero-padded to 8192 points; frame

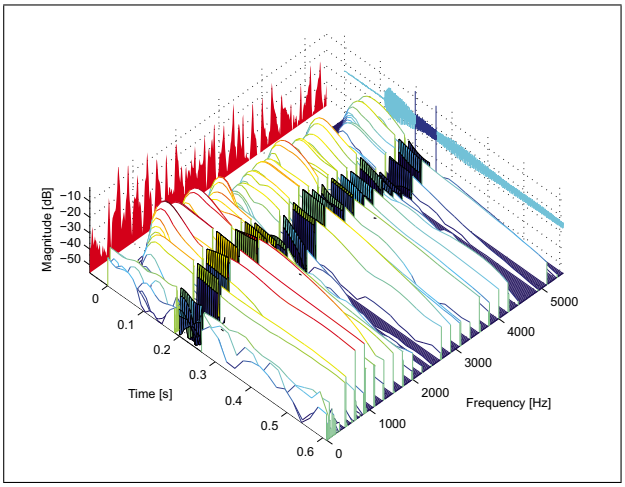

Figure A1. Spectrogram of a Shanghai A3 (221 Hz) string recording, 0-5 kHz. The time domain waveform is projected onto the right axis plane; the time interval marked between vertical lines is chosen for the spectral analysis. The corresponding spectrum of the analyzed interval is projected onto the left axis plane.

overlap of 7936 points). A time interval beginning about 100ms after the peak intensity (as shown in the waveform projected onto the right hand axis plane in Figure A1) was chosen for the analysis to reduce the influence of pluck transients on the spectrum. The analysis spectrum (projected onto the left hand axis plane in Figure A1) was constructed by taking the maxima of successive frames covering an interval of approximately 50ms, in order to recover peaks which were otherwise obscured by beating. Finally, a peak-picking algorithm was applied to calculate the center frequencies of each prominent spectral peak in order to estimate the frequency of each partial. The same procedure was repeated for each recording.

The spectrum in Figure 5 shows two features which required special consideration in the peak-picking algorithm: a missing fundamental [15] and the presence of phantom partials [16]. As can be seen in the spectrum in Figure 5, a number of local spectral peaks occur away from the expected partial frequencies. These are believed to be phantom partials, which occur in many stringed instruments, such as the piano, guitar [16] and potentially any other plucked or struck stringed instrument in which significant coupling between string, bridge, and soundboard/resonator exists[17, 18]. As a prominent example from the top panel of Figure 5, the peak at approximately 3470 Hz (between the 15^{th} and 16^{th} partials) is consistent with even phantom partial, as it is double the frequency of the eighth partial.

To accommodate these features, the peak-picking algorithm was manually initialized to start searching for peaks at low multiples of the expected fundamental frequency. In order to handle phantom partials and spurious noise, the peak picking algorithm followed a heuristic which assumed the partials were approximately locally evenly spaced, so established a search window for each successive partial computed from the average interval spacing of the previous n partials. In the case of multiple local maxima within the search window, if the signal to noise ratio in that region exceeded a predefined threshold, the largest magnitude peak was selected. [16] notes that phantom partials occasionally have larger magnitudes than typical inharmonic partials, which may explain some of the spurious points generated by the algorithm and visible in the plots, particularly at high frequencies where the signal approaches the noise floor. Final results were visually checked using diagnostic plots similar to Figure 5.

Acknowledgement

The authors thank Professor C. H. Chue, Professor Julius O. Smith, Wilson F. Chin, Tseng-Jung Chueh, and Fan-Chia Wang for assisting in this project.

References

[1] S. Sadie, G. Grove: The new Grove dictionary of music and musicians / edited by Stanley Sadie. 2nd ed. Grove, London, 2001, 29 v. (various pagings).

[2] H. Fletcher, E. D. Blackham, R. Stratton: Quality of piano tones. The Journal of the Acoustical Society of America **34** (1962) 749–761.

[3] J. Bensa: Analyse et synthese de sons de piano par modeles physiques et de signaux. Dissertation. l'Université de la Mediterranée, May 2003.

[4] Y. P. Zhuang: Pipa shou ce [pipa handbook]. Shanghai Music Publisher, Shanghai, 2001.

[5] J. E. Myers: The way of the pipa: Structure and imagery in Chinese lute music. Kent State University Press, Kent, Ohio, 1992.

[6] B. E. Anderson, W. J. Strong: The effect of inharmonic partials on pitch of piano tones. The Journal of the Acoustical Society of America **117** (2005) 3268–3272.

[7] H. Järveläinen, T. Verma, V. Välimäki: Perception and adjustment of pitch in inharmonic string instrument tones. Journal of New Music Research **31** (2002) 311–319.

[8] C. Erkut, M. Karjalainen, P. Huang, V. Välimäki: Acoustical analysis and model-based sound synthesis of the kantele. The Journal of the Acoustical Society of America **112** (2002) 1681–1691.

[9] V. Välimäki, H. Penttinen, J. Knif, M. Laurson, C. Erkut: Sound synthesis of the harpsichord using a computationally efficient physical model. EURASIP Journal on Applied Signal Processing **2004** (2004) 934–948.

[10] H. Penttinen, J. Pakarinen, V. Välimäki, M. Laurson, H. Li, M. Leman: Model-based sound synthesis of the guqin. The Journal of the Acoustical Society of America **120** (2006) 4052–4063.

[11] H. Järveläinen, M. Karjalainen: Perceptibility of inharmonicity in the acoustic guitar. Acta Acustica united with Acustica **92** (September/October 2006) 842–847(6).

[12] H. A. Conklin, Jr.: Design and tone in the mechanoacoustic piano. Part I. Piano hammers and tonal effects. The Journal of the Acoustical Society of America **99** (1996) 3286–3296.

[13] D. Rocchesso, F. Scalcon: Bandwidth of perceived inharmonicity for physical modeling of dispersive strings. Speech and Audio Processing, IEEE Transactions on **7** (1999) 597–601.

[14] K. F. Graff: Wave motion in elastic solids. Oxford University Press, 1975.

[15] J. R. Pierce: The science of musical sound. Scientific American Library, New York, 1983.

[16] H. A. Conklin, Jr.: Piano strings and "phantom" partials. The Journal of the Acoustical Society of America **102** (1997) 659–659.

[17] H. A. Conklin, Jr.: Generation of partials due to nonlinear mixing in a stringed instrument. The Journal of the Acoustical Society of America **105** (1999) 536–545.

[18] B. Bank, L. Sujbert: Generation of longitudinal vibrations in piano strings: From physics to sound synthesis. The Journal of the Acoustical Society of America **117** (2005) 2268–2278.